

One-step method for the fabrication of pure and metal-decorated densified CNT films for effective electromagnetic interference shielding

Fan Yang^a, Shengcun Ma^a, Chia Miang Khor^a, Yiming Su^a, Zahra Barani^b, Zhenpeng Xu^a, Arthur Boyko^c, Arpita Iddya^a, Naama Segev-Mark^c, Xiaoyu (Rayne) Zheng^{a,f}, Fariborz Kargar^b, Alexander A. Balandin^b, Guy Ramon^c, Igor De Rosa^{d,e}, Eric Hoek^{a,f,h,i}, David Jassby^{a,f,h,*}

^a Department of Civil & Environmental Engineering, University of California, Los Angeles (UCLA), Los Angeles, 90095, USA

^b Department of Electrical and Computer Engineering, University of California, Riverside (UCR), Riverside, 92521, USA

^c Department of Civil & Environmental Engineering, Technion – Israel Institute of Technology, Haifa, 32000, Israel

^d Institute for Carbon Management, University of California, Los Angeles (UCLA), Los Angeles, 90095, USA

^e Materials Science and Engineering, University of California, Los Angeles (UCLA), Los Angeles, 90095, USA

^f California NanoSystem Institute, UCLA, Los Angeles, 90095, USA

^g Institute of the Environment & Sustainability, UCLA, Los Angeles, 90095, USA

ⁱ Energy Storage & Distributed Resources Division, Lawrence Berkeley National Lab, Berkeley, 94720, USA

ARTICLE INFO

Keywords:

Carbon nanotube film
Electrical conductivity enhancement
Electromagnetic interference shielding

ABSTRACT

Light-weight, thin, and robust electromagnetic shielding materials with high electrical conductivity are needed for advanced modern electronics and telecommunication technologies to protect circuits from electromagnetic interference. Carbon nanotubes (CNT) are ideal candidates for electromagnetic shielding materials due to their excellent mechanical strength, high electrical conductivity, and light weight. However, the relatively poor electrical conductivity of CNT films, a result of the many points of contact resistance between neighboring CNTs, is an obstacle towards their utilization as a shielding material. Here, we propose a facile CNT film fabrication method that enhances the conductivity of CNT films by collapsing the separation between neighboring CNTs (i.e., densifying the material) in the CNT network. The dense CNT films resulting from this facile method exhibit high electrical conductivity ($\sim 10^6 \text{ S m}^{-1}$), and achieve excellent shielding of 99.999992% (71 dB) at frequencies between 8.2 GHz and 12.4 GHz with a thickness of 14.3 μm . The remarkable absolute shielding effectiveness ($3.50 \times 10^5 \text{ dB cm}^{-2} \text{ g}^{-1}$) is due to the material's low density (i.e., $\sim 1.0 \text{ g/cm}^3$), thickness (i.e., 1.3–14.3 μm), and metal-like conductivity. Also, the produced CNT sheet is an ideal substrate for gold decoration that can dramatically enhance the EMI shielding performance further (EMI SE increased from 43.90 dB in the loose film to 56.67 dB in the dense film, which further increased to 66.12 dB when the dense CNT film was coated with a thin gold layer). The outstanding properties of gold-decorated dense CNT films make them strong candidates to meet the electromagnetic shielding needs of modern cutting-edge, lightweight, and compact electronic devices.

1. Introduction

There is a critical need to attenuate electromagnetic interference (EMI) in electronic components and devices [1–3]. EMI is produced by electromagnetic fields that are generated by devices that use or transmit electricity (e.g., phones, electric vehicles, and power strips) [4]. Therefore, materials that act as a shield by reflecting and/or absorbing electromagnetic radiation producing high EMI shielding effectiveness (EMI SE) are highly desired. Development of high EMI SE materials with

easy processability, light weight, minimum thickness, and has become important due to the EMI shielding requirements of modern cutting-edge fields like aerospace materials, high-speed telecommunication and ultra-microelectronics [1,5].

Conventional metallic shielding materials, such as copper and silver, can achieve excellent EMI SE due to their intrinsically high electrical conductivity. However, their high density (e.g., 8.94 g cm^{-3} for Cu and 10.49 g cm^{-3} for Ag) and susceptibility to corrosion limits their applications as EMI shields, especially for advanced electronics [4,6].

* Corresponding author. Department of Civil & Environmental Engineering, University of California, Los Angeles (UCLA), Los Angeles, 90095, USA
E-mail address: jassby@ucla.edu (D. Jassby).

Lightweight polymer/conductive filler composites, owing to the high conductivity of the flexible fillers, such as metal wires [7–9], graphene/graphite [10–12], quasi-1D filters [13], and carbon nanotubes (CNT) have also been proposed for EMI shielding [14]. However, most polymers are insulators, and lead to poor connectivity between adjacent conductive fillers, which reduces the conductivity of the polymer composite, a critical aspect of EMI shields [14–16]. Additionally, the low durability of polymeric materials and their poor anti-bacterial properties further reduce their adoption as EMI shields in electronics [9]. In addition to polymer/filler composites, nanostructured assemblies of conductive materials like percolating networks of CNTs, reduced graphene oxide (rGO), and 2D metal carbonitrides (MXene) have also been explored as EMI shielding materials [1,4,17,18].

Individual CNTs are known to be nearly perfect molecular wires with outstanding structural, electrical, and thermal abilities [19]. The electrical conductivity of an individual CNT has been determined to be as high as $2 \times 10^7 \text{ S m}^{-1}$ [20], with a tensile strength of up to 150 GPa [21, 22]. However, poor nanoscale contacts and high junction resistance between neighboring CNTs in a percolating network undermine the electrical and mechanical properties, as well as the EMI shielding performance of CNT films. As a result, typical CNT films exhibit ~1% of their potential electrical conductivity and tensile strength compared to an individual CNT [23–25]. This poor electrical conductivity of CNT films has limited their use as a shielding material. Chlorosulfonic acid (CSA) is known as an excellent solvent and functionalization agent for the dispersal and sulfonation of CNTs [26,27]. Taking advantage of these properties, researchers have been using CSA to densify CNT network using a rather complex sequence of steps: 1) the CNT network is thermally annealed (to remove amorphous carbon impurities), 2) the CNT network is soaked in sulfuric acid to further remove residual metallic catalysts, 3) the CNT network is then soaked in CSA, and allowed to dry, which produces the densified film [28]. Although these membranes display strong EMI shielding properties, the cost (i.e. the energy required for thermal annealing, additional sulfuric acid consumption), and complexity of the treatment processes (i.e. the need to first make a loose CNT network and multiple physical and chemical processing steps) limit its potential for larger scale applications. In this study, we use a facile one-step fabrication method based on the evaporation of CNT-acid suspensions to produce a metal-like conductive CNT film for EMI shielding. Furthermore, the densified CNT network serves as an excellent substrate for the facile decoration with gold particles (or other metals), leading to further enhancement of the film's conductivity and electromagnetic interference (EMI) shielding properties. The difference in Fermi levels between Au (III) and CNT facilitates the rapid and simultaneous reduction of Au (III) to Au(0) on the densified CNT network, contributing to these improved properties [29]. While previous studies have demonstrated a multi-step process towards the same goals, here we demonstrate a highly simplified and scalable fabrication method that results in a material whose EMI shielding exceed materials fabricated using previously reported methods [26,28]. Specifically, CNTs suspended in CSA are spread over a substrate and the CSA is evaporated, which results in a densified, highly conductive thin-film

material with uniform properties and excellent EMI shielding properties (Fig. 1). In contrast, previous methods used to produce densified CNT films relied on multi-step processes. Other methods include the pre-alignment of CNTs using a rotating drum followed by the spraying and evaporation of ethanol; the produced film had a strength of 9.6 GPa with a thickness of 120 nm after further physical compression, but the authors did not describe the electrical properties of the material [21]. Other methods based on CNT arrays (i.e. CNT forests grown on the substrate) by domino-pushing (i.e. physically pushing down a CNT forest followed by compression), shear pressing, and dry drawing have also been used to produce CNT films with good mechanical strength and reasonable electrical properties [30–32]. Aligned CNT films fabricated via domino pushing had an electrical conductivity of $2.0 \times 10^4 \text{ S m}^{-1}$ compared to that of $1.5 \times 10^4 \text{ S m}^{-1}$ for random oriented samples [30]; CNT films with a thickness of 40 μm produced from shear pressing exhibited a conductivity of $1.18 \times 10^4 \text{ S m}^{-1}$ parallel to the CNT axis and $0.42 \times 10^4 \text{ S m}^{-1}$ perpendicular to the CNT axis, and a tensile strength of 402 MPa [31]; thin densified CNT sheets with a thickness of 50 nm made by dry drawing showed a conductivity of $2.86 \times 10^4 \text{ S m}^{-1}$ along the aligned CNT direction, and a tensile strength ranging between 87.5 MPa and 232.5 MPa, depending on the degree of alignment [32]. In general, all previous fabrication methods either involved a multi-step process or resulted in films with relatively poor electrical properties that would minimize their usefulness as EMI shields. The one-step CNT densification method in this study has a greater potential for scale-up, is more sustainable in terms of energy and chemical consumption, and produces an ultra-conductive, strong, and highly EMI shielding material.

2. Experimental section

2.1. Materials

Carboxyl group functionalized single-walled CNT (SWNT-COOH) with a diameter of 1–4 nm was purchased from Cheap Tubes Inc. (USA). Concentrated sulfuric acid (H_2SO_4), Sodium hydroxide (NaOH, 10 N), sodium dodecylbenzene sulfonate (SDS), and Dimethylformamide (DMF) were purchased from Fisher-Scientific. CSA and lime soda were purchased from Sigma-Aldrich. Polysulfone UF membranes (PS35, molecular weight cut-off of 20 kDa) were kindly provided by Solecta Membranes (USA). Tetrachloroauric(III) acid trihydrate ($\text{HAuCl}_4 \bullet 3\text{H}_2\text{O}$, 99.9%) was purchased from Sigma Aldrich.

2.2. Fabrication of dense CNT film

Dense CNT films with various thicknesses were prepared via a thermal-induced evaporation process by varying the amount of CNTs in a CNT/CSA suspension. A 1 g L^{-1} CNT/CSA solution was prepared by dispersing 10 mg of CNTs into 10 ml CSA in a glass vial. The CNTs/CSA dispersion was stirred mildly for 3 h on a stir plate at room temperature, prior to being poured onto a glass petri dish on a heating plate. The glass petri dish with CNT/CSA solution was then covered with a funnel, which acted as a vapor guide. The emanating vapors were directed into a gas

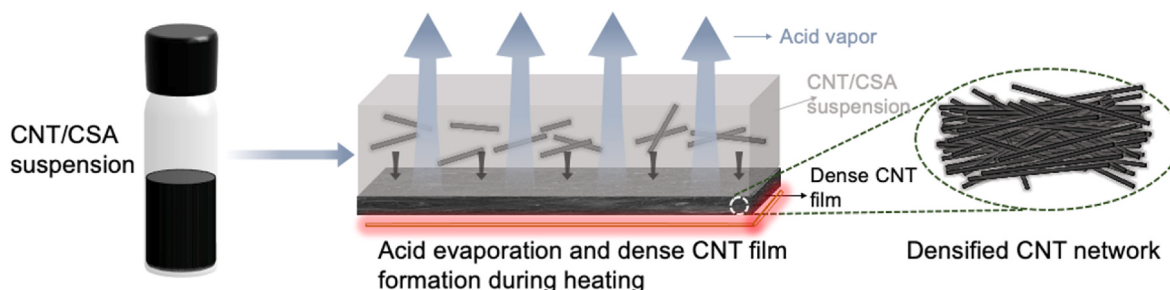


Fig. 1. Schematic diagram of dense CNT film fabrication process. (A colour version of this figure can be viewed online.)

washing bottle, containing lime soda, via the funnel using a vacuum. At the beginning of the thermal-assisted evaporation process, the temperature of the heating plate was controlled at 100 °C, which is below the boiling point of CSA (around 150 °C). As the glass petri dish heated up, the acidic vapor emanating from the CNT/CSA suspension was absorbed and neutralized by lime soda in the gas washing bottle. The subsequent evaporation of CSA led to the formation of the CNT film; the temperature was then switched to 140 °C for 0.5 h to remove any residual acid present in the CNT film. Finally, the prepared CNT film was washed thoroughly by placing the petri dish with the dense CNT film into a water bath.

2.3. Preparation of CNTs film by pressure-assisted filtration

In order to fabricate CNT film on polymeric support, 1g CNT was suspended in 1L of deionized water together with 10 g of SDS as surfactant. This CNT suspension was then sonicated with a probe ultrasonicator (120C, Branson, USA) in an ice water bath for 30 min (1s on, 1s off) followed by centrifugation for 15 min at 14,000 rpm three times to remove unsuspended particulates. 45 ml of this CNT stock solution was then pressure-deposited on a porous PS35 UF membrane at 40 psi. The prepared CNT-coated UF membrane was washed thoroughly with 1 L of deionized water to flush out the nonattached surfactant and dried at 80 °C for 30 min.

2.4. Fabrication of free-standing filter-deposited porous CNT film

To obtain the free-standing porous CNT film from the PS35 support membrane, the CNT coated- UF membrane was first rinsed in a warm DMF bath until the PS35 support separated from the CNT film layer. The CNT film was then thoroughly washed in another DMF bath, followed by soaking in a water bath. Finally, the produced free-standing CNT film was dried at 80 °C for 30 min prior to characterization.

2.5. Acid/alkali treatment of dense CNT film

1 mol L⁻¹ H₂SO₄ and 1 mol L⁻¹ NaOH solution were prepared out of concentrated H₂SO₄ and 10 N NaOH, respectively. The dense CNT films were rinsed in the prepared 1 mol L⁻¹ acid bath or 1 mol L⁻¹ alkali solution bath for 1 h. The treated dense CNT films were then thoroughly washed with DI water followed by drying at 80 °C for 30 min.

2.6. Fabrication of dense CNT/Gold film

A 20 mM gold ion solution was prepared by adding 0.157 g Tetra-chloroauric (III) acid trihydrate to 20 ml deionized water followed by sonication for 2 min. The dense CNT film was soaked in the gold ion solution in a glass jar for 20 min to complete the reduction of Au³⁺ to Au⁰: AuCl₄⁻ + 3e⁻ ↔ Au + 4Cl⁻. The reduction of Au³⁺ to Au⁰ is enabled by the difference in the Fermi levels of the CNTs and Au(III) (+0.5 V compared to the standard hydrogen electrode (SHE) for CNTs, vs. +1.002V vs. SHE for AuCl₄) [29,33]. Subsequently, the SWCNT film was taken out from the solution and washed thoroughly with deionized water. The densified gold-coated SWCNT (CNT/gold) film was then dried in an oven at 80 °C overnight and smoothed using mechanical rolling, where the CNT/gold membrane was first wet with ethanol and then rolled several times between two rollers running in opposite directions with different gaps (from 10 μm to 5 μm).

2.7. Materials characterization

The electrical conductivity of films was calculated from their sheet resistance using a 4-point-probe conductivity meter (MCP-T610, Mitsubishi Chemical Analytech Co., Japan). The film morphology and the cross-sectional structure were studied using a scanning electron microscope (SEM) (Zeiss SUPRA 40-VP) and Nova 600 SEM/FIB system,

respectively. Contact angle measurements were performed using a contact angle goniometer (250-U1, rame-hart instrument co., USA). The chemical composition of the CNT film's surface was determined using X-ray photon spectroscopy (XPS) (Kratos Axis Ultra DLD spectrometer equipped with a monochromatic Al K α X-ray source). XPS data was processed using CasaXPS software (version 2.3.18). The tensile strength of CNT films was tested using a ~5 mm × 25 mm strip. Unidirectional tensile tests were performed using Instron 5944 with a 500 N load cell to evaluate the corresponding stress-strain curves (Reference standard: ASTM – D882). A strain rate of 10⁻³ s⁻¹ was applied on each sample until fracture. The effective stiffness was calculated by testing linearity via the least-squares regression technique. X-ray diffraction (XRD) measurements were performed on a Panalytical X'Pert Pro X-ray powder diffractometer (Malvern Panalytical, Netherlands) using Cu K α 1 radiation under double axis diffraction condition. The step size of the 2θ-ω scans was 0.02° and the scan speed time was 0.1°/s.

2.8. Electromagnetic interference shielding measurement

Evaluation of EMI shielding performance in X-band frequency range of CNT films was carried out using a vector network analyzer (VNA) (N5247A, Agilent, USA) via the coaxial method. The samples were cut into a 25 mm × 12 mm strip to fit the waveguide window (22.86 mm × 10.16 mm). Before data collection, two working ports of the VNA were calibrated using the standard SSLT method. For each experiment, scattering parameters (S11, S22, S12, and S21) were recorded for EMI SE calculation.

2.9. Theoretical calculations of EMI shielding effectiveness

EMI SE (dB) displays the ability of a material to attenuate the incident EM waves. The total EMI SE (SE_T) is composed of three components: reflection shielding (SE_R), absorption shielding (SE_A), and multiple reflections shielding (SE_M). Generally, the SE_M can be neglected when the SE_T is larger than 15 dB [3].

$$SE_T = SE_R + SE_A + SE_M \quad (2)$$

In order to calculate the SE_T, SE_R, and SE_A, reflectivity (R) and transmission (T) values need to be obtained from their coefficients (r and t, respectively) in terms of scattering parameters.

$$R = |r|^2 = |S_{11}|^2 \quad (3)$$

$$T = |t|^2 = |S_{12}|^2 \quad (4)$$

SE_T, SE_R, and SE_A can further be calculated as follows

$$SE_T = 10 \log \left(\frac{1}{T} \right) = 10 \log \left(\frac{1}{|t|^2} \right) \quad (5)$$

$$SE_R = 10 \log \left(\frac{1}{1 - R} \right) = 10 \log \left(\frac{1}{1 - |r|^2} \right) \quad (6)$$

$$SE_A = 10 \log \left(\frac{1 - R}{T} \right) = 10 \log \left(\frac{1 - |r|^2}{|t|^2} \right) \quad (7)$$

Calculation of Absolute Shielding Effectiveness: prior to calculating the absolute shielding effectiveness, specific shielding effectiveness (SSE) is required. SSE is defined by normalizing shielding effectiveness with the density (SE/density, dB cm³ g⁻¹). Absolute shielding effectiveness is then calculated by dividing SSE with the thickness (SSE/t), taking both density and thickness of materials into account: SSE/t = SE/(density·t) (dB cm² g⁻¹).

3. Results and discussion

Reducing the contact resistance by decreasing the distance between individual CNTs can significantly improve the conductive performance of CNT networks since the intrinsic resistance of CNTs is negligible compared to contact resistance between neighboring CNTs in a network (i.e., resistance caused by electron tunneling) [34,35]. The facile fabrication process of the metal-like CNT film is illustrated in Fig. 1. CSA, a true solvent of CNTs, exhibits the highest solubility of individual CNTs, where CNTs are well dispersed (i.e. in an isotropic phase) when their concentrations are below 0.61 vol% [26]. The highly polar CSA is capable of polarizing

(Fig. 2a). Low concentration CNT dispersions in CSA exhibit an isotropic phase with random orientation [27]. However, as the concentration increases, the CNTs transition into a liquid-crystalline (LC) phase, where the CNTs become densely packed and aligned due to excluded volume effects [26]. Between these extreme conditions (i.e., medium concentrations), a biphasic phase of CNTs is formed [26]. CSA, a true solvent of CNTs, exhibits the highest solubility of individual CNTs, where CNTs are well dispersed (i.e. in an isotropic phase) when their concentrations are below 0.61 vol% [26]. The highly polar CSA is capable of polarizing

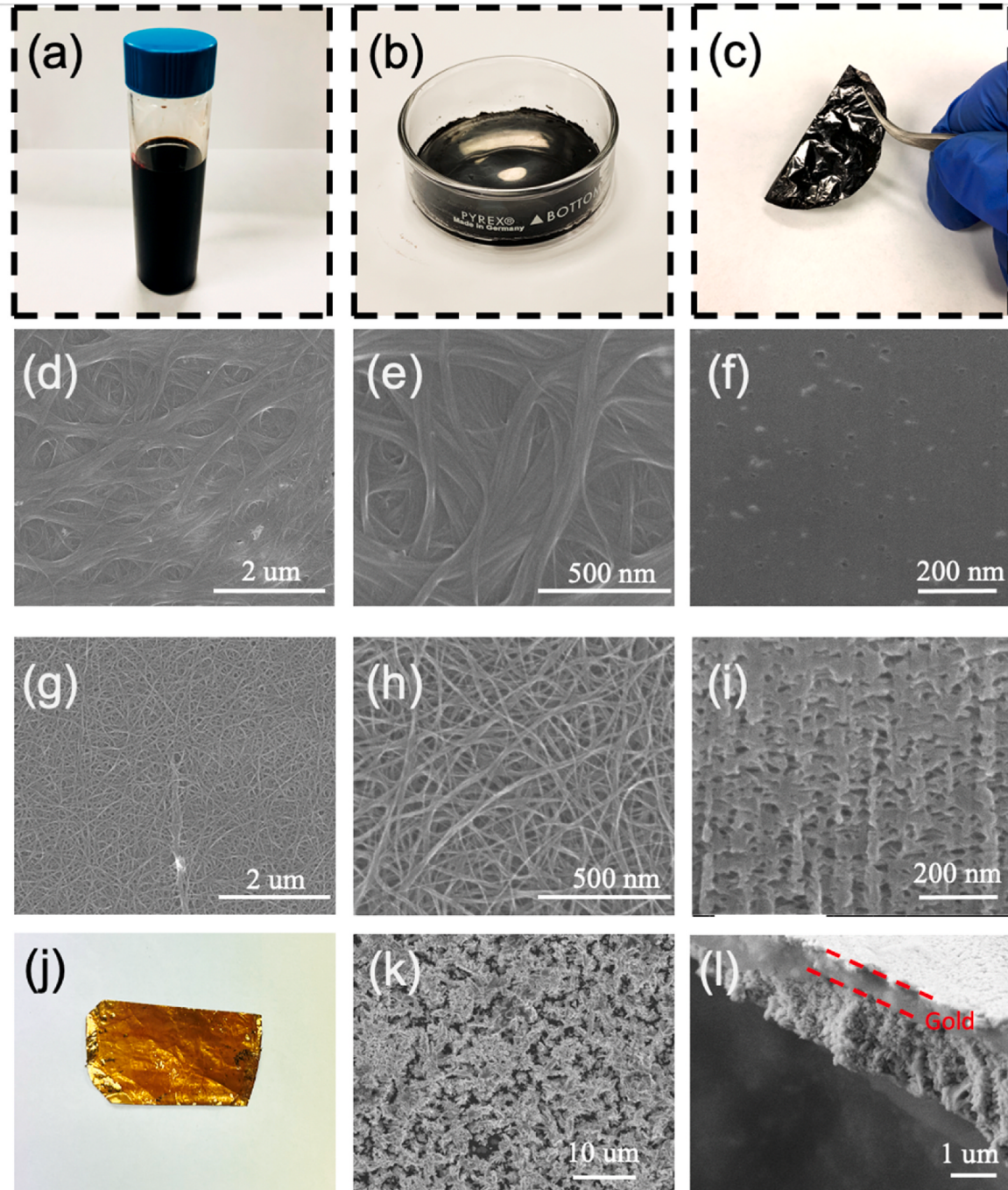


Fig. 2. (a) CNT/CSA suspension in glass vial. (b), (c) Light - reflecting dense CNT films with patches of light reflecting off: (b) Photo of dense CNT film in glass petri dish after evaporation of CSA, (c) photo of free-standing dense CNT film peeled from petri dish. (d), (e) Low-magnification (d) and high-magnification (e) SEM images of surface morphology of dense CNT film. (f) SEM image of dense CNT film from cross-sectional view. (g), (h) Low-magnification (g) and high-magnification (h) SEM images of surface morphology of a pressure-deposited porous CNT film. (i) SEM image of a pressure-deposited porous CNT film from cross-sectional view. (j) photo of dense CNT coated with gold. (k) SEM image of the surface of dense CNT film coated with gold. (l) Cross-sectional view of dense CNT film with gold coating. (A colour version of this figure can be viewed online.)

individual CNTs, enhancing the attractive forces between adjacent polarized CNTs [28]. As a result, when the CSA evaporates, the CNT network collapses and forms a dense film (Fig. 2b). The dense CNT film has a metallic, reflective appearance, reflecting light off of the surface (Fig. 2b and c). The dense CNT film shows enhanced electrical conductivity ($0.78 \times 10^6 \pm 4.85 \times 10^4 \text{ S m}^{-1}$), which is two orders of magnitude higher than traditional CNT-based films (i.e., $\sim 10^4 \text{ S m}^{-1}$) [36], and comparable to conductive metals (e.g., $\sim 1 \times 10^6 \text{ S m}^{-1}$ for stainless steel) [37]. A pressure-deposited porous CNT film was used as a comparison with the dense CNT film in terms of conductivity and morphology. The surface of dense CNT films was imaged using scanning electron microscopy (SEM), and shows individual CNT and CNT bundles tightly packed with no observable gaps between them (Fig. 2d and e). Cross-sectional images of the dense CNT film show the dense structure of CNT network and the close packing of CNTs (Fig. 2f). In contrast, porous CNT films fabricated by pressure-depositing a CNT/surfactant suspension show a very loose CNT network with large pores between neighboring CNTs (Fig. 2g–i). The porous structure of the film was also observable in a cross-sectional image of the material (Fig. 2i). When the dense CNT membrane was coated with gold and mechanically rolled, a shiny metallic golden is obtained (Fig. 2j). Initially, the CNTs, acting as electron donors, reduce Au (III) ions in the solution to metal Au, resulting in the formation of gold clusters on the surface of the CNT film and within the porous film. As these gold clusters grow larger and form a continuous layer, they interlock with the CNT network at the interface. The interlocking mechanism involves the interplay of van der Waals forces, which contribute to the interfacial interactions and subsequently influence the mechanical properties of the film. After the mechanical compaction process, the separation distance between the two layers at

the interface and between the gold particles decreases. This closer proximity enhances the van der Waals forces, both between the layers and among the gold particles. These strengthened van der Waals forces contribute to improved interfacial adhesion and cohesion. SEM image analysis reveals a crystal-like gold layer on the surface of the densified CNT network. (Fig. 2k-l).

The electrical conductivity of the dense CNT film was a function of its thickness, with the highest conductivity ($0.78 \times 10^6 \pm 4.85 \times 10^4 \text{ S m}^{-1}$) measured at a film thickness of $2.8 \mu\text{m}$ (Fig. 3a); this value is ~ 2.7 times higher than that of a non-densified, porous CNT film ($2.92 \times 10^5 \pm 1.11 \times 10^4 \text{ S m}^{-1}$) (Fig. 3a, and Table S1). The conductivity of the CNT/gold membrane with a total thickness of $3.3 \mu\text{m}$ increased to $2.31 \times 10^6 \pm 3.60 \times 10^4 \text{ S m}^{-1}$, a nearly 8-fold increase compared to the non-densified CNT film. At a low thickness of $1.3 \mu\text{m}$, a small amount of CNTs within a certain volume may not form a tightly packed film. Consequently, the uneven distribution of CNTs can result in regions with fewer CNTs compared to other regions. These low-density regions, characterized by large gaps between CNT individuals/bundles, can introduce additional resistance when the thickness is small [38]. However, as the thickness increases, the number of these low density regions declines and the conductivity of the CNT network stops increasing with thickness, stabilizing at $0.78 \times 10^6 \text{ S m}^{-1}$ at $2.8 \mu\text{m}$. XRD spectrum analysis demonstrates the successful growth of Au on the dense CNT network (Fig. 3b): the diffraction peaks at 38.4° , 44.6° , 64.7° , 77.71° , and 81.85° can be assigned to (111), (200), (220), (311), and (222) crystalline diffraction planes of Au. Au diffraction peaks correspond to the typical face-centered cubic crystal structure and does not indicate the presence of any intermetallic gold compounds. Furthermore, the Au (111) peak exhibits strong intensity compared to those of Au (200), Au

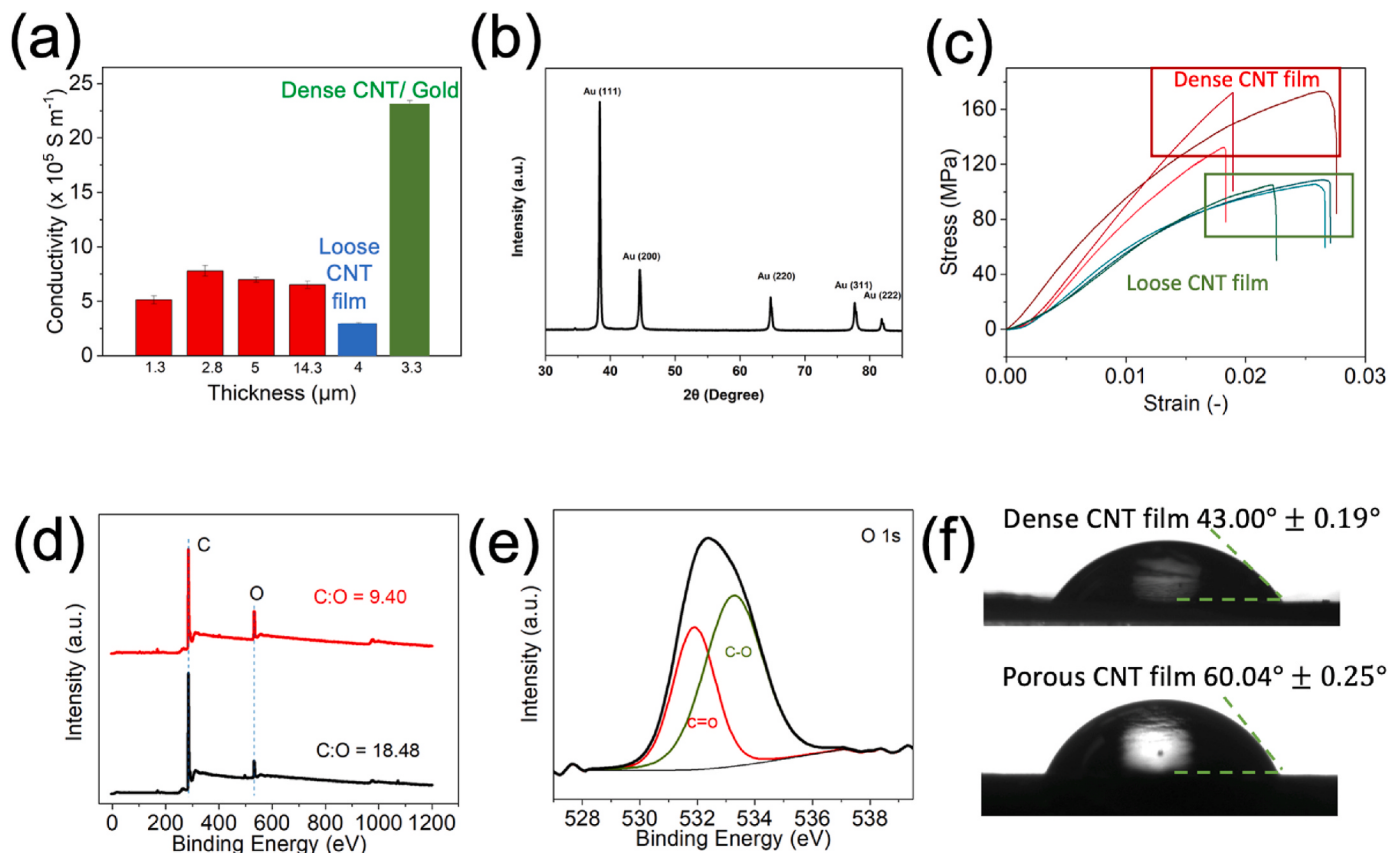


Fig. 3. (a) Changes in electrical conductivity of dense CNT films as a function of thickness (red), compared with porous CNT films (blue). (b) XRD spectrum of dense CNT/Au film. (c) Stress – strain curve of dense CNT films (red) and porous CNT films (blue) with a thickness of $2.8 \mu\text{m}$. (d) XPS survey spectra of a dense CNT film (red line) and porous CNT film (black line). (e) High resolution spectra of O 1s of a dense CNT film. (f) Water contact angle measurements of a dense and porous CNT film. (A colour version of this figure can be viewed online.)

(220), and Au (311) planes. The relative intensity of Au (200)/Au (111) is 0.27, lower than the bulk gold value (0.52 from JCPDS #04-0784), indicating the synthesized Au film were highly (111) oriented [39].

The high conductivity of the dense CNT film is a result of the dense

CNT network that reduced the resistance to electron transport between neighboring CNTs, which is highly sensitive to the separation distance between conducting strands in a network [30,40,41]. In contrast, for the pressure-deposited CNT film, the large gaps between neighboring CNTs

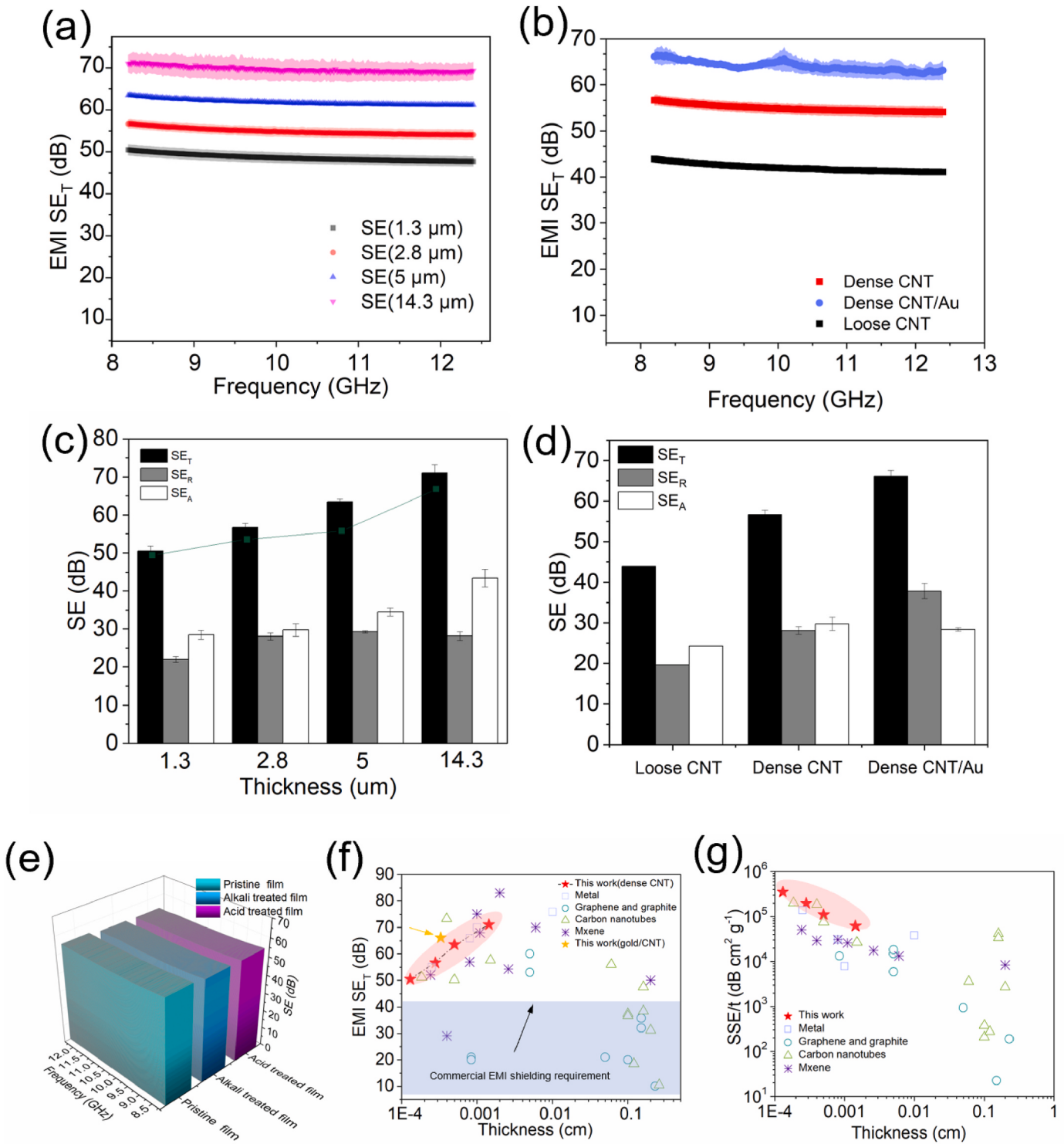


Fig. 4. (a) Variances of total SE_T over X band for dense CNT films with different thicknesses (1.3 μm , 2.8 μm , 5 μm , and 14.3 μm). (b) SE_T over X band for loose CNT film, dense CNT film, and dense CNT/Au film. (c) Measured SE_T , calculated SE_T from Simon's formula, and measured absorption (SE_A) and reflection (SE_R) in dense CNT films at 8.2 GHz. (d) Measured SE_T , SE_A , and SE_R for loose CNT film, dense CNT film, and dense CNT/Au film. (e) SE_T of pristine dense CNT film, acid treated CNT film, and alkali treated CNT film over X band. (f) Comparison of EMI SE_T with the previously published data of metals, graphene and graphite, Carbon nanotube, and MXenes. (g) Comparison of absolute SE with the previously published data of metals, graphene and graphite, Carbon nanotube, and MXenes. (A colour version of this figure can be viewed online.)

(Fig. 2h) increased the electron hopping distance and reduced the membrane conductivity.

The mechanical strength of the CNT films, evaluated from the tensile stress-strain curves, showed that the dense CNT films had enhanced mechanical properties (Fig. 3c). Specifically, the ultimate strength of the dense CNT film, calculated by dividing the applied force by the cross-sectional area of the film, was 161.5 ± 25.6 MPa at $2.16 \pm 0.52\%$ deformation. In contrast, the ultimate strength and maximum deformation of the porous CNT film were 106.6 ± 2.0 MPa and $2.54 \pm 0.25\%$, respectively. The ultimate strength of the dense CNT film (161.5 MPa) is 1.52 times higher than that of a porous CNT film because the CSA-induced densification shortens the separation distance. As a result, the attractive van der Waals force between adjacent CNTs is enhanced [42], and the dense CNT network shows stronger mechanical properties. Based on the stress and strain values at failure, the Young's modulus of dense and porous films was calculated to be 10.85 ± 0.67 GPa and 6.99 ± 0.25 GPa, respectively (details in Table S2). The ultimate strength of a dense CNT film was found to be higher than that of aluminum (~ 110 MPa). However, its stiffness is much lower than that of aluminum (~ 69 GPa), suggesting that this light-weight film has superior mechanical strength and excellent flexibility. Additionally, the film can be folded and twisted without any damage, as shown in Supporting Information.

X-ray photoelectron spectroscopy (XPS) survey spectra of a dense and porous CNT film exhibited sharp peaks associated with C and O, originating from the carbonous CNT backbone and surface functional groups (Fig. 3d). After CSA evaporation, the C/O ratio of dense CNT film was 9.40, lower than the 18.48 ratio found on porous films, which can be attributed to the partial oxidation of CNTs by the strong acid CSA. A high-resolution XPS scan of O1s shows that the ratio of C=O/C – O for the dense CNT film is 0.61, while the C=O/C – O ratio is only 0.35 for a porous CNT film (Fig. 3e and Fig. S2). The larger number of C=O groups in the dense CNT film further supports the observation that the immersion of the CNTs in CSA led to the oxidation of surface carbon groups. The oxidation of dense CNT film is also evident through the contact angle measurements of the porous and dense films (Fig. 3f). The contact angle of a porous film ($60.0 \pm 0.3^\circ$) was determined to be higher than that of a dense CNT film ($43.0 \pm 0.2^\circ$). The lower contact angle of the dense CNT film suggests the presence of more polar surface groups, which can be attributed to the oxidation of carbon groups (e.g., carboxyl and carbonyl groups). It is indeed worth noting that the conductivities of dense CNT films exhibit an increase, even when the individual CNTs within them are oxidized (as shown in Fig. 3a). Generally, CNTs without any defects tend to possess higher conductivity compared to CNTs with functional groups [43]. However, in the case of the dense CNT film, the overall conductivity increase can be attributed to the decrease in contact resistance, which arises from the densification of the CNT network, which more than offsets the decrease in conductivity resulting from the CNT oxidation.

Due to their dense structure, intrinsically high electrical conductivity and multiple functional groups, dense CNT films show exceptionally high EMI SE values. Fig. 4a shows the total EMI shielding effectiveness (SE_T) of a dense CNT film with different thicknesses (1.3 μm, 2.8 μm, 5 μm, and 14.3 μm) over the X-band frequency range (8.2 GHz–12.4 GHz). It is noted that SE_T increased with an increase in film thickness. Yet, even the thinnest dense film (1.3 μm) has a SE_T of 50.5 ± 1.3 dB, and demonstrates ~99.999% blockage of incident EM waves, which is higher than the commercial EMI shielding requirement (40 dB) [44]. The SE_T reaches as high as 71 ± 2.1 dB with a film thickness of 14.3 μm, suggesting that 99.999992% of EM waves are attenuated by the dense CNT film. Compared with the loose CNT film, the dense CNT film's SE_T was 12.77 dB higher at same thickness (i.e. 2.8 μm) (Fig. 4b). The dense CNT/Au films shows a further enhancement of EMI SE compared to the uncoated dense film; the EMI SE over the whole X band was lifted by 22.22 dB after the Au coating, reaching a value of 66.12 dB for a dense CNT/Au film (the total thickness of new CNT/gold film is 3.3 μm) (Fig. 4b). To deconvolute the SE_T value in terms of the EMI shield's

properties, we used Simon's formula [45]:

$$SE_T = 50 + 10 \log(\sigma / f) + 1.7t(\sigma f)^{0.5} \quad (1)$$

where σ , f , and t represent electrical conductivity ($S \text{ cm}^{-1}$), frequency (MHz), and thickness of the EMI shield (cm), respectively. The first two terms of the equation represent shielding due to reflection, while the third term accounts for shielding from absorption; multireflection is neglected in this equation. From Simon's formula, the overall shielding performance of a CNT film can be enhanced by either increasing the electrical conductivity or thickness. As shown in Fig. 4c, the calculated SE_T values from Simon's formula follow the same trend as the measured SE_T values, which increase with an increase in thicknesses.

To identify the mechanism responsible for the observed EMI shielding in the dense CNT film, the contributions from absorption (SE_A), reflection (SE_R), and multi-reflection (SE_M , which is generally negligible when the SE_T is larger than 15 dB) [3] are determined and compared (Fig. 4c). As mentioned earlier, it has been observed that the SE_T tends to increase with an increase in thickness. In the case of the films under investigation SE_A values consistently surpass SE_R values across all thicknesses. This finding suggests that absorption plays a more prominent role in determining the EMI shielding capability of dense CNT films within the range of 1.3–14.3 μm. Interestingly, SE_R increases from 22 dB (at 1.3 μm) to 28 dB (at 2.8 μm), but does not continue to increase beyond this thickness. In contrast, SE_A continuously increases with thickness. This can be attributed to the differences between the reflection and absorption processes. Specifically, the incident EM waves first hit the conductive surface of the shielding material where over 99% (20 dB) of the EM waves are instantly reflected due to the impedance mismatch [11,46]. The residual energy (<1%) of the EM waves can penetrate the material, but is attenuated throughout the depth of the film. These penetrated waves are either directly absorbed by ohmic losses [5], due to the occurrence of EM field-induced current that produces thermal energy [47,48], or reflected at first and then absorbed by adjacent CNTs. In other words, the reflection of EM waves is mainly impacted by a film's electrical conductivity, while EM wave absorption happens throughout the material leading to an increase in absorption with an increase of thickness. A material's electrical conductivity has a large impact on SE_R and SE_A values, albeit to a different degree, as implied from Simon's formulism, Eq. (1), which partially explains why SE_A grows more than SE_R . SE_R is proportional to the logarithm of the material's electrical conductivity, while SE_A is proportional to the square root of the conductivity. Therefore, changes in conductivity have bigger impacts on SE_A than on SE_R . In addition to the excellent conductivity, polar functional groups, such as C–O and C=O, the presence of which was verified using XPS analysis (Fig. 3d), can also contribute to the high SE_R through polarization losses [17]. In Fig. 4d, we conducted a comparison of the SE in terms of SE_T , SE_R , SE_A among the loose CNT film, dense CNT film, and dense CNT/Au film. The loose CNT film exhibited inferior performance in both SE_A and SE_R compared to the dense CNT film and dense CNT/Au film. This can be attributed to its relatively lower conductivity, resulting in a smaller SE_T value. On the other hand, the dense CNT/Au film demonstrated the highest SE_T and SE_R among the three films, while SE_A was comparable to that of the dense CNT film. Specifically, the SE_T and SE_R increased by 9.5 dB and 9.7 dB, respectively, while SE_A stabilized at around 29 dB. This suggests that the increase in SE_T was primarily driven by the increase in reflection provided by the gold coating, as gold is well-known for its excellent reflective properties [49]. In our two-layer nanostructured composite, the thin top layer (the Au(0)) with high conductivity primarily serves as a means to reflect EM waves upon initial contact. This layer efficiently redirects the waves away from the material. On the other hand, the thicker secondary nanostructured layer (the CNTs) is designed to absorb and disperse the residual waves that penetrate the top layer. The secondary layer acts as a prolonged pathway for the waves, allowing for multiple reflections and ensuring further attenuation of the EMI. By

combining the reflective properties of the thin top layer with the absorbing and multi-reflective capabilities of the thicker secondary layer, the composite provides an effective solution for EMI shielding [50]. As a result, the majority of EM waves (37.8 dB) were reflected by highly conductive dense CNT/gold top surface, the remaining attenuated wave was absorbed and dissipated within the CNT layer.

The dense CNT film exhibited robust stability under harsh conditions. The SE_T of dense CNT film remained constant after a 1-h immersion in acid (1 M H_2SO_4 solution) or base (1 M $NaOH$ solution) over the X-band frequency range (Fig. 4e). The high stability of these dense CNT films makes them superior to traditional metallic or polymeric shielding materials that are vulnerable to harsh conditions [51].

The EMI SE_T values of our dense CNT film and dense CNT/gold film were compared to values reported for other materials (Fig. 4f and Table S3). In general, carbon-based materials, such as CNTs, graphene, and graphite, are generally found in the right lower corner of Fig. 4f, indicating that they can only achieve a sufficient SE_T at fairly large thicknesses (500 μm –1000 μm), due to their low electrical conductivity. Although metal materials show similar EMI shielding properties compared to our dense CNT films, the high density and poor processibility of metals (i.e., fabricating them into super thin films) limit their application as EM shields for advanced electrical devices. In contrast, the dense 14.3 μm thick CNT film in this work displays an extraordinary EMI SE_T of 71 dB, and is not inferior to MXenes with a similar thickness in terms of EMI shielding [4]. The gold/CNT film shows an excellent EMI SE_T of 66.12 dB with 3.3 μm thickness, which outperforms almost all of the materials we have been studied at such a low thickness.

The absolute shielding effectiveness (SSE/t , $dB \text{ cm}^2 \text{ g}^{-1}$) of the dense CNT films is compared to that of other materials, with the SSE/t value being calculated by dividing SE_T by the product of the material density and thickness (Fig. 4g) [45]. A higher SSE/t value suggests that a given material could achieve a specific SE with a lighter weight and a lower thickness. The dense CNT film shows an impressive SSE/t value that outperforms those exhibited by highly electrically conducting metals and MXenes. The highest value of SSE/t of $3.6 \times 10^5 \text{ dB cm}^2 \text{ g}^{-1}$ was achieved at a thickness of 1.3 μm , where the SE is 50.5 dB, which is higher than that required for commercial devices (40 dB) [1]. The ability to achieve high SE at low thicknesses and light weight makes dense CNT films an excellent candidate as an EMI shielding material for modern advanced electronics and telecommunication devices.

4. Conclusions

In conclusion, we have reported a CNT film fabrication method that produces metal-like CNT films with robust mechanical strength (161.5 MPa), chemical stability, and high electrical conductivity (779,500 $S \text{ m}^{-1}$) for carbon-based materials. In addition to its impressive electrical conductivity, the rich functional groups on the dense CNT film contribute to high EMI SE with a very low thickness (i.e., 71 dB at 14.3 μm). With the addition of the gold coating, the dense CNT/gold membrane exhibits an extremely high conductivity ($2.31 \times 10^6 \text{ S m}^{-1}$) and EMI SE of 66.12 dB at a total thickness of 3.3 μm . Furthermore, the dense CNT films are highly stable under harsh conditions and maintain excellent shielding performance after acid/alkali treatment, suggesting their promising potential use in advanced electrical and telecommunication devices.

CRediT authorship contribution statement

Fan Yang: Conceptualization, experimental work, Formal analysis, writing. **Shengcun Ma:** Experimental work, Formal analysis. **Chia Miang Khor:** Experimental work, Formal analysis. **Yiming Su:** Experimental work, Formal analysis. **Zahra Barani:** Experimental work, Formal analysis. **Zhenpeng Xu:** Experimental work, Formal analysis. **Arthur Boyko:** Experimental work, Formal analysis. **Arpita Iddy:** Experimental work, Formal analysis. **Naama Segev-Mark:** Formal

analysis. **Xiaoyu (Rayne) Zheng:** Supervision. **Fariborz Kargar:** Experimental work, Formal analysis. **Alexander A. Balandin:** Supervision. **Guy Ramon:** Supervision. **Igor De Rosa:** Experimental work, Formal analysis, Supervision. **Eric Hoek:** Supervision, Conceptualization, Writing – review & editing. **David Jassby:** Supervision, Conceptualization, Writing – review & editing.

Declaration of competing interest

The authors declare that they have no known competing financial interests or personal relationships that could have appeared to influence the work reported in this paper.

Acknowledgment

The authors acknowledge financial support from the National Science Foundation (1926360). In addition, the authors would like to thank the Center for High Frequency Electronics (CHFE) and Minji Zhu for assistance with the vector network analyzer instrument. Additional support for EMVH was provided by the *UCLA Sustainable LA Grand Challenge*. A.A.B acknowledges the support of the Vannevar Bush Faculty Fellowship (VBFF), under contract ONR-N00014-21-1-2947.

Appendix A. Supplementary data

Supplementary data to this article can be found online at <https://doi.org/10.1016/j.carbon.2023.118370>.

References

- [1] A. Iqbal, F. Shahzad, K. Hantanasisarakul, M.-K. Kim, J. Kwon, J. Hong, H. Kim, D. Kim, Y. Gogotsi, C.M. Koo, Anomalous absorption of electromagnetic waves by 2D transition metal carbonitride Ti3CNTx (MXene), *Science* 369 (6502) (2020) 446–450.
- [2] M. Han, C.E. Shuck, R. Rakhmanov, D. Parchment, B. Anasori, C.M. Koo, G. Friedman, Y. Gogotsi, Beyond Ti3C2Tx: MXenes for electromagnetic interference shielding, *ACS Nano* 14 (4) (2020) 5008–5016.
- [3] P. Sambyal, A. Iqbal, J. Hong, H. Kim, M.K. Kim, S.M. Hong, M. Han, Y. Gogotsi, C. M. Koo, Ultralight and mechanically robust Ti3C2Tx hybrid aerogel reinforced by carbon nanotubes for electromagnetic interference shielding, *ACS Appl. Mater. Interfaces* 11 (41) (2019) 38046–38054.
- [4] F. Shahzad, M. Alhabeb, C.B. Hatter, B. Anasori, S.M. Hong, C.M. Koo, Y. Gogotsi, Electromagnetic interference shielding with 2D transition metal carbides (MXenes), *Science* 353 (6304) (2016) 1137–1140.
- [5] Z. Zhou, J. Liu, X. Zhang, D. Tian, Z. Zhan, C. Lu, Ultrathin MXene/calcium alginate aerogel film for high-performance electromagnetic interference shielding, *Adv. Mater. Interfac.* 6 (6) (2019).
- [6] S.H. Lee, S. Yu, F. Shahzad, W.N. Kim, C. Park, S.M. Hong, C.M. Koo, Density-tunable lightweight polymer composites with dual-functional ability of efficient EMI shielding and heat dissipation, *Nanoscale* 9 (36) (2017) 13432–13440.
- [7] S. Lin, H. Wang, F. Wu, Q. Wang, X. Bai, D. Zu, J. Song, D. Wang, Z. Liu, Z. Li, Room-temperature production of silver-nanofiber film for large-area, transparent and flexible surface electromagnetic interference shielding, *npj Flexible Electronics* 3 (1) (2019) 1–8.
- [8] G.A. Gelves, M.H. Al-Saleh, U. Sundararaj, Highly electrically conductive and high performance EMI shielding nanowire/polymer nanocomposites by miscible mixing and precipitation, *J. Mater. Chem.* 21 (3) (2011) 829–836.
- [9] Z. Zeng, F. Jiang, Y. Yue, D. Han, L. Lin, S. Zhao, Y.B. Zhao, Z. Pan, C. Li, G. Nystrom, J. Wang, Flexible and ultrathin waterproof cellular membranes based on high-conjunction metal-wrapped polymer nanofibers for electromagnetic interference shielding, *Adv. Mater.* 32 (19) (2020), e1908496.
- [10] D.Q. Zhang, T.T. Liu, J.C. Shu, S. Liang, X.X. Wang, J.Y. Cheng, H. Wang, M.S. Cao, Self-Assembly construction of WS2-rGO architecture with green EMI shielding, *ACS Appl. Mater. Interfaces* 11 (30) (2019) 26807–26816.
- [11] Y. Lin, J. Dong, H. Zong, B. Wen, H. Yang, Synthesis, characterization, and electromagnetic wave absorption properties of composites of reduced graphene oxide with porous LiFeSO₄ microspheres, *ACS Sustain. Chem. Eng.* 6 (8) (2018) 10011–10020.
- [12] Y. Li, X. Pei, B. Shen, W. Zhai, L. Zhang, W. Zheng, Polyimide/graphene composite foam sheets with ultrahigh thermostability for electromagnetic interference shielding, *RSC Adv.* 5 (31) (2015) 24342–24351.
- [13] Z. Barani, F. Kargar, Y. Ghafouri, S. Ghosh, K. Godziszewski, S. Baraghani, Y. Yashchyshyn, G. Cywinski, S. Rumyantsev, T.T. Salguero, A.A. Balandin, Electrically insulating flexible films with quasi-1D van der Waals fillers as efficient electromagnetic shields in the GHz and sub-THz frequency bands, *Adv. Mater.* 33 (11) (2021), e2007286.

- [14] I.W. Nam, H.K. Lee, J.H. Jang, Electromagnetic interference shielding/absorbing characteristics of CNT-embedded epoxy composites, *Compos. Appl. Sci. Manuf.* 42 (9) (2011) 1110–1118.
- [15] M.H. Al-Saleh, U. Sundararaj, Electromagnetic interference shielding mechanisms of CNT/polymer composites, *Carbon* 47 (7) (2009) 1738–1746.
- [16] Y. Yang, M.C. Gupta, K.L. Dudley, R.W. Lawrence, Novel carbon nanotube–polystyrene foam composites for electromagnetic interference shielding, *Nano Lett.* 5 (11) (2005) 2131–2134.
- [17] B. Wen, M. Cao, M. Lu, W. Cao, H. Shi, J. Liu, X. Wang, H. Jin, X. Fang, W. Wang, J. Yuan, Reduced graphene oxides: light-weight and high-efficiency electromagnetic interference shielding at elevated temperatures, *Adv. Mater.* 26 (21) (2014) 3484–3489.
- [18] B. Shen, W. Zhai, W. Zheng, Ultrathin flexible graphene film: an excellent thermal conducting material with efficient EMI shielding, *Adv. Funct. Mater.* 24 (28) (2014) 4542–4548.
- [19] M.S. Mauter, M. Elimelech, Environmental applications of carbon-based nanomaterials, *Environ. Sci. Technol.* 42 (16) (2008) 5843–5859.
- [20] T. Ebbesen, H. Lezec, H. Hiura, J. Bennett, H. Ghaemi, T. Thio, Electrical conductivity of individual carbon nanotubes, *Nature* 382 (6586) (1996) 54–56.
- [21] W. Xu, Y. Chen, H. Zhan, J.N. Wang, High-strength carbon nanotube film from improving alignment and densification, *Nano Lett.* 16 (2) (2016) 946–952.
- [22] M.-F. Yu, O. Lourie, M.J. Dyer, K. Moloni, T.F. Kelly, R.S. Ruoff, Strength and breaking mechanism of multiwalled carbon nanotubes under tensile load, *Science* 287 (5453) (2000) 637–640.
- [23] W.A. Deheer, W.S. Bacsa, A. Chatelain, T. Gerfin, R. Humphreybaker, L. Forro, D. Ugarte, Aligned carbon nanotube films - production and optical and electronic properties, *Science* 268 (5212) (1995) 845–847.
- [24] E. Belyarova, M.E. Itkis, N. Cabrera, B. Zhao, A.P. Yu, J.B. Gao, R.C. Haddon, Electronic properties of single-walled carbon nanotube networks, *J. Am. Chem. Soc.* 127 (16) (2005) 5990–5995.
- [25] J. Stallard, W. Tan, F. Smail, T. Gspann, A. Boies, N. Fleck, The mechanical and electrical properties of direct-spun carbon nanotube mats, *Extreme Mechanics Letters* 21 (2018) 65–75.
- [26] V.A. Davis, A.N. Parra-Vasquez, M.J. Green, P.K. Rai, N. Behabtu, V. Prieto, R. D. Booker, J. Schmidt, E. Kesselman, W. Zhou, H. Fan, W.W. Adams, R.H. Hauge, J. E. Fischer, Y. Cohen, Y. Talmon, R.E. Smalley, M. Pasquali, True solutions of single-walled carbon nanotubes for assembly into macroscopic materials, *Nat. Nanotechnol.* 4 (12) (2009) 830–834.
- [27] O. Kleinerman, L. Liberman, N. Behabtu, M. Pasquali, Y. Cohen, Y. Talmon, Direct imaging of carbon nanotube liquid-crystalline phase development in true solutions, *Langmuir* 33 (16) (2017) 4011–4018.
- [28] Y.J. Wan, X.Y. Wang, X.M. Li, S.Y. Liao, Z.Q. Lin, Y.G. Hu, T. Zhao, X.L. Zeng, C. H. Li, S.H. Yu, P.L. Zhu, R. Sun, C.P. Wong, Ultrathin densified carbon nanotube film with “Metal-like” conductivity, superior mechanical strength, and ultrahigh electromagnetic interference shielding effectiveness, *ACS Nano* 14 (10) (2020) 14134–14145.
- [29] H.C. Choi, M. Shim, S. Bangsaruntip, H. Dai, Spontaneous reduction of metal ions on the sidewalls of carbon nanotubes, *J. Am. Chem. Soc.* 124 (31) (2002) 9058–9059.
- [30] D. Wang, P. Song, C. Liu, W. Wu, S. Fan, Highly oriented carbon nanotube papers made of aligned carbon nanotubes, *Nanotechnology* 19 (7) (2008), 075609.
- [31] P.D. Bradford, X. Wang, H. Zhao, J.-P. Maria, Q. Jia, Y. Zhu, A novel approach to fabricate high volume fraction nanocomposites with long aligned carbon nanotubes, *Compos. Sci. Technol.* 70 (13) (2010) 1980–1985.
- [32] M. Zhang, S. Fang, A.A. Zakhidov, S.B. Lee, A.E. Aliev, C.D. Williams, K. R. Atkinson, R.H. Baughman, Strong, transparent, multifunctional, carbon nanotube sheets, *Science* 309 (5738) (2005) 1215–1219.
- [33] A.E. Goldt, O.T. Zaremba, M.O. Bulavskiy, F.S. Fedorov, K.V. Larionov, A. P. Tsapenko, Z.I. Popov, P. Sorokin, A.S. Anisimov, H. Inani, J. Kotakoski, K. Mustonen, A.G. Nasibulin, Highly efficient bilateral doping of single-walled carbon nanotubes, *J. Mater. Chem. C* 9 (13) (2021) 4514–4521.
- [34] C. Li, E.T. Thostenson, T.-W. Chou, Dominant role of tunneling resistance in the electrical conductivity of carbon nanotube-based composites, *Appl. Phys. Lett.* 91 (22) (2007).
- [35] K.Y. Yan, Q.Z. Xue, Q.B. Zheng, L.Z. Hao, The interface effect of the effective electrical conductivity of carbon nanotube composites, *Nanotechnology* 18 (25) (2007).
- [36] G. Chen, D.N. Futaba, S. Sakurai, M. Yumura, K. Hata, Interplay of wall number and diameter on the electrical conductivity of carbon nanotube thin films, *Carbon* 67 (2014) 318–325.
- [37] K.A. Ibrahim, B. Wu, N.P. Brandon, Electrical conductivity and porosity in stainless steel 316L scaffolds for electrochemical devices fabricated using selective laser sintering, *Mater. Des.* 106 (2016) 51–59.
- [38] M.L. Erickson, S.M. Elliott, C.J. Brown, P.E. Stackelberg, K.M. Ransom, J.E. Reddy, C.A. Cravotta 3rd, Machine-learning predictions of high arsenic and high manganese at drinking water depths of the glacial aquifer system, northern continental United States, *Environ. Sci. Technol.* 55 (9) (2021) 5791–5805.
- [39] W. Xin, J.-M. Yang, C. Li, M.S. Goorsky, L. Carlson, I.M. De Rosa, Novel strategy for one-pot synthesis of gold nanoparticles on carbon nanotube sheet as an effective flexible SERS substrate, *ACS Appl. Mater. Interfaces* 9 (7) (2017) 6246–6254.
- [40] B.J. Hinds, N. Chopra, T. Rantell, R. Andrews, V. Gavalas, L.G. Bachas, Aligned multiwalled carbon nanotube membranes, *Science* 303 (5654) (2004) 62–65.
- [41] B.J. Hinds, N. Chopra, T. Rantell, R. Andrews, V. Gavalas, L.G. Bachas, Aligned multiwalled carbon nanotube membranes, *Science* 303 (5654) (2004) 62–65.
- [42] P. Goh, A. Ismail, B. Ng, Directional alignment of carbon nanotubes in polymer matrices: contemporary approaches and future advances, *Compos. Appl. Sci. Manuf.* 56 (2014) 103–126.
- [43] A. Nish, R.J. Nicholas, Temperature induced restoration of fluorescence from oxidised single-walled carbon nanotubes in aqueous sodium dodecylsulfate solution, *Phys. Chem. Chem. Phys.* 8 (30) (2006) 3547–3551.
- [44] L.-C. Jia, D.-X. Yan, Y. Yang, D. Zhou, C.-H. Cui, E. Bianco, J. Lou, R. Vajtai, B. Li, P.M. Ajayan, Z.-M. Li, High strain tolerant EMI shielding using carbon nanotube network stabilized rubber composite, *Advanced Materials Technologies* 2 (7) (2017).
- [45] T. Yun, H. Kim, A. Iqbal, Y.S. Cho, G.S. Lee, M.K. Kim, S.J. Kim, D. Kim, Y. Gogotsi, S.O. Kim, C.M. Koo, Electromagnetic shielding of monolayer MXene assemblies, *Adv. Mater.* 32 (9) (2020), e1906769.
- [46] H. Xu, X. Yin, M. Zhu, M. Han, Z. Hou, X. Li, L. Zhang, L. Cheng, Carbon hollow microspheres with a designable mesoporous shell for high-performance electromagnetic wave absorption, *ACS Appl. Mater. Interfaces* 9 (7) (2017) 6332–6341.
- [47] Y. Wan, P. Xiong, J. Liu, F. Feng, X. Xun, F.M. Gama, Q. Zhang, F. Yao, Z. Yang, H. Luo, Y. Xu, Ultrathin, strong, and highly flexible Ti₃C₂Tx MXene/bacterial cellulose composite films for high-performance electromagnetic interference shielding, *ACS Nano* 15 (5) (2021) 8439–8449.
- [48] Q. Song, F. Ye, X. Yin, W. Li, H. Li, Y. Liu, K. Li, K. Xie, X. Li, Q. Fu, L. Cheng, L. Zhang, B. Wei, Carbon nanotube-multilayered graphene edge plane core-shell hybrid foams for ultrahigh-performance electromagnetic-interference shielding, *Adv. Mater.* 29 (31) (2017).
- [49] J. Li, H. Liu, J. Guo, Z. Hu, Z. Wang, B. Wang, L. Liu, Y. Huang, Z. Guo, Flexible, conductive, porous, fibrillar polymer–gold nanocomposites with enhanced electromagnetic interference shielding and mechanical properties, *J. Mater. Chem. C* 5 (5) (2017) 1095–1105.
- [50] B. Zhou, G. Han, Z. Zhang, Z. Li, Y. Feng, J. Ma, C. Liu, C. Shen, Aramid nanofiber-derived carbon aerogel film with skin-core structure for high electromagnetic interference shielding and solar-thermal conversion, *Carbon* 184 (2021) 562–570.
- [51] Y. Wang, X. Jing, Intrinsically conducting polymers for electromagnetic interference shielding, *Polym. Adv. Technol.* 16 (4) (2005) 344–351.